Available online at www.sciencedirect.com
SCIENCE DIRECT®
ELSEVIER
Ocean Engineering 33 (2006) 1322–1342
OCEAN ENGINEERING
www.elsevier.com/locate/oceaneng

Computational and experimental study on performance of sails of a yacht

Jaehoon Yoo [a,1], Hyoung Tae Kim [b,*]

[a] *Marine Transportation Systems Research Division, Korea Ocean Research and Development Institute, 171 Jang-dong, Yuseong-gu, Daejeon 305-343, South Korea*
[b] *Department of Naval Architecture and Ocean Engineering, Chungnam National University, 220 Gung-dong, Yuseong-gu, Daejeon 305-764, South Korea*

Received 1 February 2005; accepted 4 August 2005
Available online 10 November 2005

Abstract

It is important to understand flow characteristics and performances of sails for both sailors and designers who want to have efficient thrust of yacht. In this paper the viscous flows around sail-like rigid wings, which are similar to main and jib sails of a 30 feet sloop, are calculated using a CFD tool. Lift, drag and thrust forces are estimated for various conditions of gap distance between the two sails and the center of effort of the sail system are obtained. Wind tunnel experiments are also carried out to measure aerodynamic forces acting on the sail system and to validate the computation. It is found that the combination of two sails produces the lift force larger than the sum of that produced separately by each sail and the gap distance between the two sails is an important factor to determine total lift and thrust.

Keywords: Sailing yacht; Interaction; Gap distance; CFD; RANS; Wind tunnel

1. Introduction

The sailing performance of a yacht depends on the balance of hydro- and aero-dynamic forces acting on the hull and on the sails. The sail tuning, i.e. direction of sail, sail shaping and gap distance between sails, etc. should be altered to meet oncoming wind in

* Corresponding author. Tel.: +82 42 821 6629; fax: +82 42 823 5437.
E-mail addresses: jhyoo@kriso.re.kr (J. Yoo), h-tkim@cnu.ac.kr (H.T. Kim).
[1] Tel.: +82 42 868 7242; fax: +82 42 868 7274.

0029-8018/$ - see front matter
doi:10.1016/j.oceaneng.2005.08.008

Nomenclature

I	height of the upper end of the forestay above the sheer
J	horizontal distance from the forestay at the sheer to the forward side of mast
P	mainsail hoist, band to band or mainsail halyard sheave top to top of boom
E	after side of mast to boom end or mainsail clew limit band on the boom
H	height of sail from sail foot
C	chord length
Φ	mast angle (angle between vessel centerline and sail chord line)
Φ_0	mast angle at sail foot
f	camber of sail section
A	projected area of sail
S	surface area of sail (reference area for non-dimensionalization)
C_L	lift coefficient ($=\text{Lift}/1/2\rho SU_\infty^2$)
C_D	drag coefficient ($=\text{Drag}/1/2\rho SU_\infty^2$)
C_P	pressure coefficient ($=+/1/2\rho U_\infty^2$)
U_∞	inflow velocity, herein the apparent wind speed
Subscripts	
F	jib sail
M	main sail

appropriate angles to push a yacht toward a destination with best efficiency. Normally these tunings are performed by yacht drivers in sailing, but also designer should make the sails have good performance at the design stage. In order to design the efficient sail system, designer is forced to have information about the essential characteristics of sail system. This paper presents computational and experimental results for the aerodynamic forces acting on sail-like wings and the characteristics of airflows around them and as well the aerodynamic interactions between jib and main sails.

In the present study, CFD techniques simulating turbulent flows around two sails are utilized. It is the merit of CFD application that it can provide not only global quantities like sail forces and moments but also detailed flow information useful for the design of a sail system. CFD can also save a lot of efforts in measuring the global quantities and detailed flow information at the towing tank or in the wind tunnel, although the computed results may not give accurate and reliable values as in the experiment. It is believed that CFD is the cost-effective tool for the performance prediction of a sailing yacht. Lee et al. (1997) have been studied on the sail interactions by CFD method and suggested that CFD is the useful tool for sail design and performance prediction of sails.

Wind-tunnel model tests were also carried out to measure lift and drag of the sail system for the present 30 feet sloop. There found are some experimental data for sailing yacht with substantial lift/drag augmentation (Wilkinson, 1989; Claughton and Campbell, 1994). On the contrary, similar studies for the sail system of relatively a small-sized sloop

are very rare. It is obvious the aero-elastic shape deformation of the sail system should be considered to predict the correct lift and drag. However, the shape deformation in general depends on seaming and rig tension, etc. and at present the scale, effect of aero-elastic deformation is not well understood. Thus, in the present study, the sail shape is fixed and assumed independent upon incoming wind, as a first approximation, in both the CFD calculation and the wind tunnel test. Using a CFD tool the viscous flows around sail-like rigid wings, which represent typical geometry of the main and jib sails of a 30 feet sloop, are calculated. In the wind tunnel test, a scaled FRP model was used to measure the forces acting on the combined sail system. Finally, CFD calculations are compared with experimental results to validate and explore the lift and drag changes due to various sail conditions.

2. Definitions of geometry

Fig. 1 shows the sail system of a 30 feet sloop for the present study, which has been developed by Kordi (Yoo et al. 2005a,b,c). A typical sail system of a sloop has jib

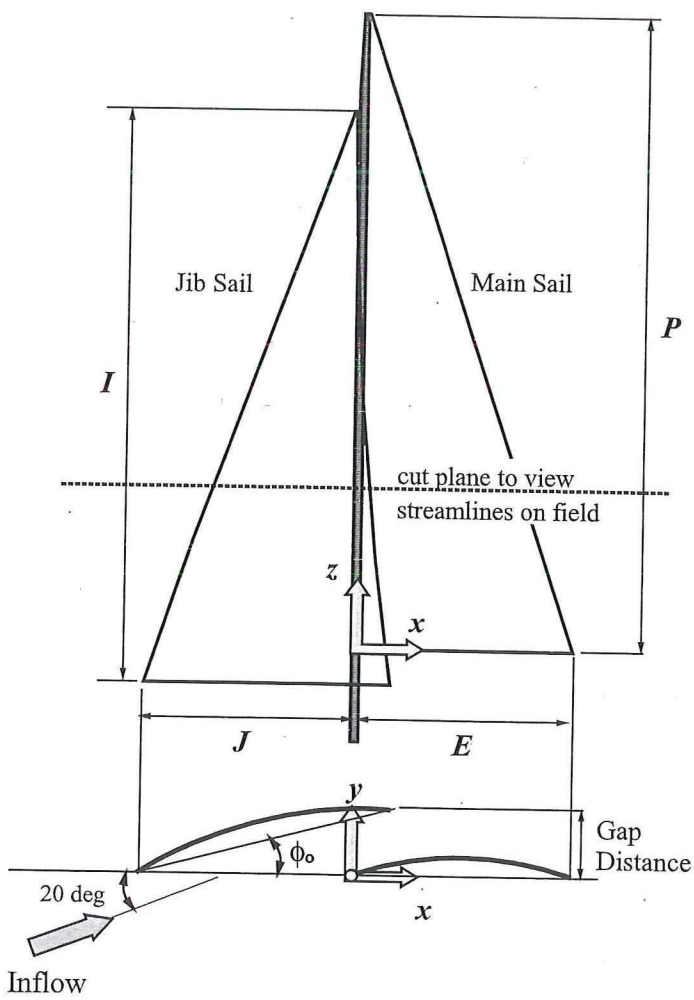

Fig. 1. Schematic view of sail system.

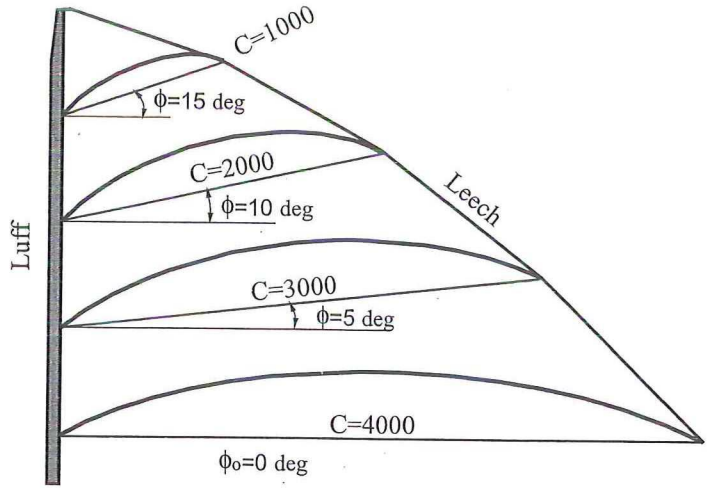

Fig. 2. Schematic view of the main sail.

and main sails and a gap distance between them is defined as the distance between the trailing edge of the jib and main sails at foot, which can be expressed alternatively by the mast angle of jib sail foot relative to the mast angle of main sail foot as shown in Fig. 1. This gap distance is one of the important parameter for the performance of the sail system as well as interactions between two sails. In this study, the shape of sail surface is expressed by a zero-thickness wing section with the NACA $a=0.8$ mean-line, as described by Abbott and Doenhoff, (1949). It is chosen mainly because of its similarity to modern cloth sails. The geometry of the sail system is defined by other parameters to reproduce realistic and actual operating conditions. Typical close-hauled sail is represented by five sections for each sail as shown in Figs. 2 and 3. For the each section of sails, typical parameters such as chord length, camber and mast angles are selected as given in Table 1 and the remaining surface of the sails between the sections are interpolated from the information on each sections. The mast angle of each section is

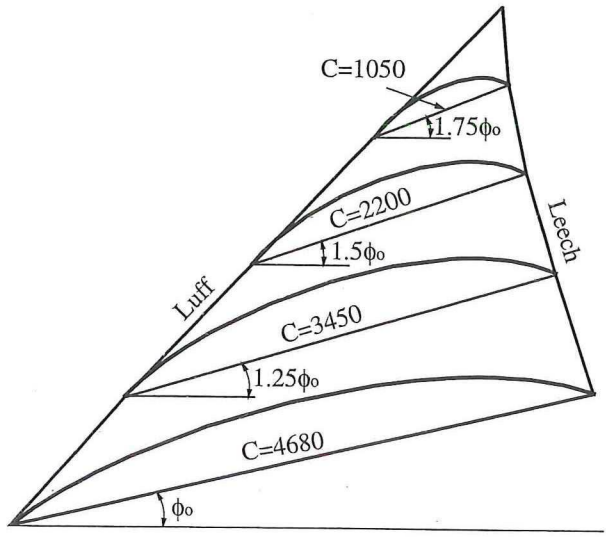

Fig. 3. Schematic view of the jib sail.

Table 1
Geometric parameters of main sail

	Foot	25%	50%	75%	Top
H (mm)	0	3000	6000	9000	11900
C (mm)	4000	3000	2000	1000	10
Φ (deg)	0	5	10	15	20
f/C (%)	8	10	12	14	16

Table 2
Geometric parameters of jib sail

	Foot	25%	50%	75%	Top
H (mm)	0	2750	5500	8250	11000
C (mm)	4680	3450	2200	1050	10
Φ (deg)	Φo	1.25Φo	1.5Φo	1.75Φo	2.0Φo
f/C (%)	8	10	12	14	16

varied to express the span-wise distribution of the sail twist. The principal dimensions of main sail are $P=11.9$ m, $E=4.0$ m, and $A_M=23.8$ m^2 with a mast of 150 mm diameter. Similarly the jib sail geometry is described by three parameters, but the mast angle of jib sail foot can be regarded as the gap distance between two sails, so those were set as the variables for each case as shown in Table 2 and Fig. 3. The principal dimensions of jib sail are $J=3.9$ m, $I=11.0$ m, and $A_F=21.5$ m^2.

CFD calculations and wind tunnel tests are carried out for the cases of three mast angles, i.e. $\Phi_0=5°$, $\Phi_0=10°$ and $\Phi_0=15°$ and the overall view of three cases of combined the sail system can be seen in Fig. 4.

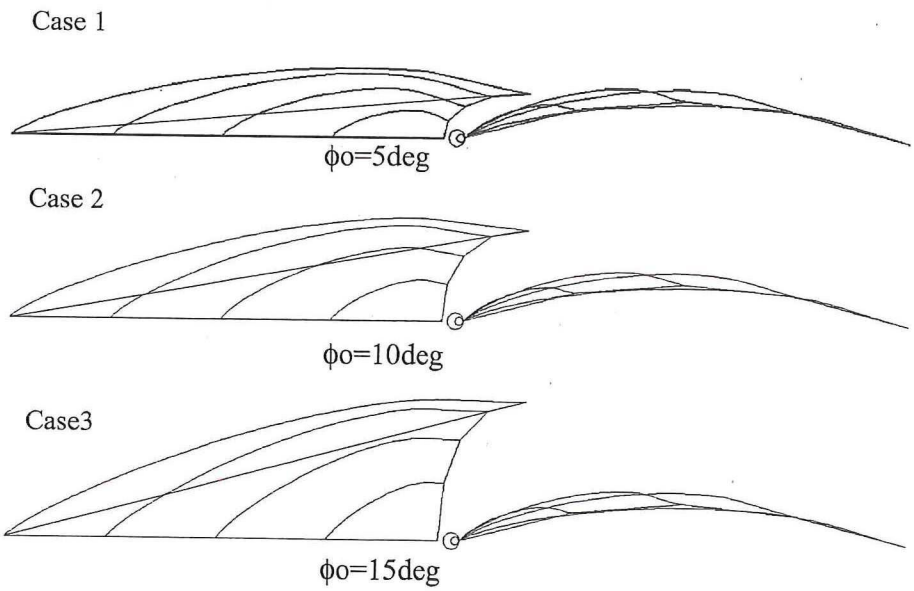

Fig. 4. Geometries of sail systems for three cases (top view). (a) top view, (b) surface mesh.

3. Computational method

In the present study, turbulent flows around the sail system of a sloop are simulated using the WAVIS code solving three-dimensional Reynolds-averaged Navier–Stokes (RANS) equations. The WAVIS code was developed at KRISO/KORDI to simulate turbulent flow around marine vehicles and extensively validated (Kim & Van, 2000; Kim et al., 2002). In the followings, the brief description of WAVIS is given. For more details, see the references.

3.1. Governing equations

The governing equations for turbulent flow in the present study are the Reynolds-averaged Navier–Stokes equations for momentum transport and the continuity equation for mass conservation. The Cartesian coordinates are used, where (x,y,z) denotes downstream, starboard, and upward direction, respectively, as shown in Fig. 1. For the non-dimensionalization, the length of main sail foot was used $(=L)$.

Continuity equation is

$$\frac{\partial u_k}{\partial x_k} = 0. \tag{1}$$

Momentum transport equations are

$$\frac{\partial u_i}{\partial t} + \frac{\partial (u_i u_j)}{\partial x_j} = -\frac{\partial p}{\partial x_i} + \frac{\partial \tau_{ij}}{\partial x_j}, \tag{2}$$

$u_i=(u,v,w)$ are the velocity components in $x_i=(x,y,z)$ directions and p the static pressure. Stress tensor τ_{ij} can be written using Boussinesq's isotropic eddy viscosity hypothesis as follows.

$$\tau_{ij} = \nu_e\left(\frac{\partial u_i}{\partial u_j} + \frac{\partial u_j}{\partial u_i}\right) - \frac{2}{3}\delta_{ij}k \tag{3}$$

Here k is the turbulent kinetic energy and ν_e the effective viscosity, defined as the sum of turbulent eddy viscosity ν_t and kinematic viscosity ν, i.e.

$$\nu_e = \nu_t + \frac{1}{\mathrm{Re}} \tag{4}$$

Re is Reynolds number $(U_\infty L/\nu)$.

For turbulence closure, the realizable k-ε model (Shih et al., 1995) is employed for the current study. In this turbulence model, the eddy viscosity ν_t can be usually written as

$$\nu_t = C_\mu \frac{k^2}{\varepsilon} \tag{5}$$

C_μ is given as the followings.

$$C_\mu = \frac{1}{A_0 + A_S \frac{U^* k}{\varepsilon}} \tag{6}$$

The parameters of the above equation are defined as

$$U^* = \sqrt{S_{ij}S_{ij} + \Omega_{ij}\Omega_{ij}}, \tag{7}$$

$$S_{ij} = \frac{1}{2}\left(\frac{\partial u_i}{\partial x_j} + \frac{\partial u_j}{\partial x_i}\right), \tag{8}$$

$$\Omega_{ij} = \frac{1}{2}\left(\frac{\partial u_i}{\partial x_j} - \frac{\partial u_j}{\partial x_i}\right), \tag{9}$$

$$A_0 = 4.0, \quad A_S = \sqrt{6}\cos\phi, \tag{10}$$

$$\phi = \frac{1}{3}\text{arc}\cos(\sqrt{6}W) \tag{11}$$

$$W = \frac{S_{ij}S_{jk}S_{ki}}{\tilde{S}^3}, \quad \tilde{S} = \sqrt{S_{ij}S_{ij}}. \tag{12}$$

The turbulent kinetic energy k can be obtained by the solution of the following transport equation.

$$\frac{\partial k}{\partial t} + \frac{\partial(u_j k)}{\partial x_j} = \frac{\partial}{\partial x_j}\left[\left(\nu + \frac{\nu_t}{\sigma_k}\right)\frac{\partial k}{\partial x_j}\right] + G - \varepsilon \tag{13}$$

Here ε represents the dissipation rate of turbulent kinetic energy and G is production term as given below.

$$G = \nu_t\left(\frac{\partial u_i}{\partial x_j} + \frac{\partial u_j}{\partial x_i}\right)\frac{\partial u_i}{\partial x_j} \tag{14}$$

The constant $\sigma_k = 1.0$ in Eq. (13).
The transport equation for dissipation rate ε is written by

$$\frac{\partial \varepsilon}{\partial t} + \frac{\partial(u_j \varepsilon)}{\partial x_j} = \frac{\partial}{\partial x_j}\left[\left(\nu + \frac{\nu_t}{\sigma_\varepsilon}\right)\frac{\partial \varepsilon}{\partial x_j}\right] + S_\varepsilon \tag{15}$$

For the realizable k-ε model,

$$S_\varepsilon = C_{\varepsilon 1} S\varepsilon - C_{\varepsilon 2}\frac{\varepsilon^2}{k + \sqrt{\nu\varepsilon}}, \tag{16}$$

In the above, $\sigma_\varepsilon = 1.2$, $C_{\varepsilon 2} = 1.9$ and

$$C_{\varepsilon 1} = \max\left(0.43, \frac{\eta}{\eta + 5}\right). \tag{17}$$

Here $\eta = Sk/\varepsilon$.

It is advisory to use a near-wall turbulence model to resolve boundary layer all the way to the wall, but then the number of grid should be almost doubled. For the present study the so-called Launder and Spalding (1974)'s wall function is utilized to bridge the fully turbulent region and the wall. The first grid point in the wall function approach is approximately 100 times off the wall compared to that in the near wall turbulence model. It provides the economy and robustness to a viscous flow calculation method as a design tool. Since the flow around yacht sails of the present interest, the so-called singular separation with flow reversal is not expected. The wall function is known to give good results for such a mild flow. The wall function adopted in the present calculation is given by

$$\frac{U_P C_\mu^{1/4} k_P^{1/2}}{\tau_w} = \frac{1}{\kappa} \ln(E n_P^*), \tag{18}$$

$$\kappa = 0.41, \tag{19}$$

$$E = 8.342, \tag{20}$$

Here τ_w is wall shear stress, U_P and k_P, respectively, the magnitude of velocity and turbulent kinetic energy at the center of the first cell off the wall. The non-dimensionalized normal distance from the wall n_P^* is given by

$$n_P^* = \frac{C_\mu^{1/4} k_P^{1/2} n_P}{\nu}. \tag{21}$$

Generation of turbulent kinetic energy at the first cell off the wall is given as follows.

$$\bar{G}_P = \tau_w \left(\frac{\partial U}{\partial n}\right)_P = \frac{\tau_w^2}{\kappa C_\mu^{1/4} k_P^{1/2} n_P}, \tag{22}$$

The dissipation at that cell is written by

$$\bar{\varepsilon}_P = \frac{C_\mu^{3/4} k_P^{3/2}}{\kappa n_P}. \tag{23}$$

3.2. Numerical discretization

The cell-centered finite-volume method is utilized to discretize the governing equations, as discussed in Ferziger and Peric (1999). Governing equations are integrated

over a grid cell Ω with boundary surface S, resulting in the following equations.

$$\int_S \vec{v}\cdot\vec{n}\mathrm{d}S = 0, \tag{24}$$

$$\frac{\partial}{\partial t}\int_\Omega u_i \mathrm{d}\Omega + \int_S u_i\vec{v}\cdot\vec{n}\mathrm{d}S = \int_S \tau_{ij}\vec{i}_j\cdot\vec{n}\mathrm{d}S - \int_S p\vec{i}_i\cdot\vec{n}\mathrm{d}S \tag{25}$$

$\vec{i}_j$ is unit vector in x_j-direction.

The first term of momentum transport equation, temporal derivative is ignored by putting very big time step, since only the steady solution is of the present interest. Convection terms are discretized using QUICK scheme of the third order. But the QUICK scheme requires 13-point stencil, resulting in complicated algebraic equations. Thus, the so-called deferred correction is adopted, which a simple upwind scheme is used with lagged higher-order terms. The deferred correction makes seven point stencil with simple linear equations. Rewriting the third term of stress tensor,

$$\int_S \tau_{ij}\vec{i}_j\cdot\vec{n}\mathrm{d}S = \int_S \nu_t\left(\frac{\partial u_i}{\partial x_j} + \frac{\partial u_j}{\partial x_i}\right)\vec{i}_j\cdot\vec{n}\mathrm{d}S = \int_S \nu_t\left(\mathrm{grad}(u_i)\cdot\vec{n} + \frac{\partial u_j}{\partial x_i}\vec{i}_j\cdot\vec{n}\right)\mathrm{d}s \tag{26}$$

Central difference scheme is utilized for diffusion terms, while the partial terms stemming from grid non-orthogonality are deferred. Linear equations obtained from seven-point stencil are solved using strongly implicit procedure (Stone, 1968).

If the pressure field is known a priori, momentum equations will give correct velocity field. However, those velocity components will not satisfy the continuity equation. To ensure divergence-free velocity field, the SIMPLEC method (Van Doormal and Raithby, 1984) is employed. Since the collocated grid arrangement is chosen, the artificial dissipation term in pressure correction equation is added, as discussed in Rhie and Chow (1983). The resulting linear equations for pressure correction are solved using strongly implicit procedure until the equation residual drops by an order of magnitude in iteration.

With a generated grid system, a flow calculation is initiated starting from uniform stream. With the grids and initial guess for flow field ready, iteration begins for coupled partial differential equations. After three momentum-transport equations are solved sequentially to obtain preliminary velocity components, the pressure correction equations are solved to get pressure field. Then, velocity components are corrected using new pressure values. Next turbulence equations are solved and eddy viscosity is updated. Iteration continues until total residuals of each momentum equation become less than 10^{-5}, which is about five orders less than the initial residuals.

4. CFD calculations

4.1. Assumptions and conditions

CFD calculations are carried out with the assumptions as follows:

(1) The mast and boom is not deformed.
(2) The vessel and sail system are not heeled but in upright condition.
(3) The surface of sail is not deformed and rigid membrane.
(4) The incident angle of apparent wind is set to 20° with respect to the mast, and the speed of wind assumed 20 knots. All forces and flow simulations are computed at the Reynolds number of 2.84×10^6, which corresponds to the wind speed of 20 knots and reference length is of main sail foot (4.0 m).

4.2. Grid generation

The grid system for CFD calculation is generated by using GridGen Package. Fig. 5 displays the grid system used for those calculations, consisting of 13 blocks with 1,796, 770 grid points. C-H type grid topology is used and the distance of the first adjacent grid from the sail surface is adjusted to $y^+=50$–230.

5. Experimental method

The experiments are carried out in the wind tunnel of the Chungnam National University of Korea. The test section dimension is 5.2 m$\times$1.8 m$\times$1.8 m and the wind speed is 45 m/s at maximum. The geometry of sails is the same as that selected for the CFD calculations. The sail model is made of fiber-glass reinforced plastics (FRP) with the scale of 1/9 and is constituted by some rigs as a boom, side shrouds, fore and after stays, which are not considered into the CFD calculations. It may be considered more accurately as sail-shaped membrane wings. Fig. 6 shows the equipped model sails in the wind tunnel. A three-component load cell is installed under the sail model with a deck-sized flat plate and some rigs as shown in Fig. 7. The experiments are carried out for wind speeds 7, 10, 12 m/s, which correspond to Reynolds numbers, 2.1×10^5, 3.0×10^5, 3.6×10^5, respectively.

6. Results and discussions

6.1. Sails without interactions

Before considering the interaction between two sails, the flow computations for each sail standing separately were carried out. Figs. 8 and 9 show limiting streamlines on the main and the jib sail surfaces with pressure coefficient Cp contours, respectively. Streamlines around sails over the section of 25% height of E (the plane to view

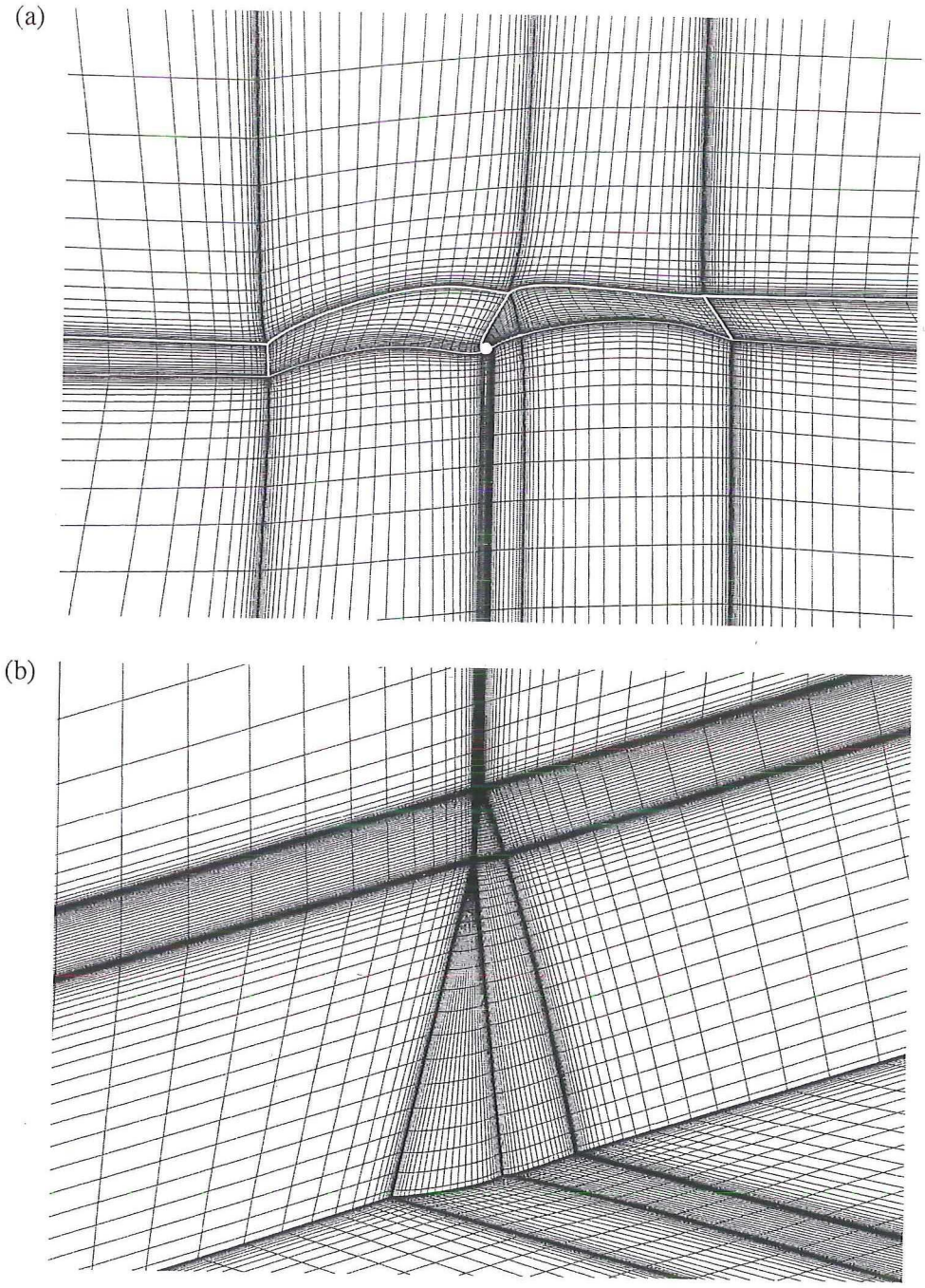

Fig. 5. Generated grid system (1,796,770 points, 13 blocks).

the streamlines on field is displayed in Fig. 1) are shown in Figs. 10 and 11. There is found no flow separation except a small region near the leech of the main sail on leeward side where the camber reduces very quickly as close to the trailing edge.

6.2. Sails with interactions

In case that two sails are set in close proximity, it is expected the interaction between two sails results in two prominent flow alterations: (a) there will be a pattern of downwash

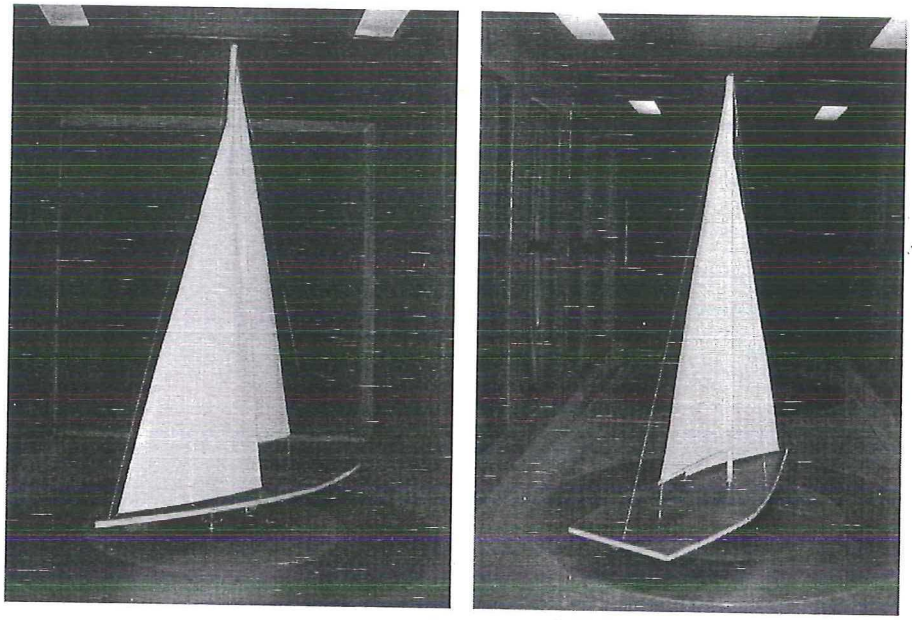

Fig. 6. Model sails in wind tunnel.

or upwash generated by each sail, which will operate in an airflow modified by the presence of the other sail and (b) when the gap between two sails is sufficiently small, the fore sail guides the flow on to the leading edge of the trailing sail and modifies the pattern of flow separation on the trailing sail, which is similar to the nozzle flow or Venturi effect (Claughton et al., 1998). Fig. 12 shows the streamlines around the sail on the section of 25% height of E. As the gap distance reduces, the angle of attack of the jib sail increases and the flow separation on leeward side of the jib sail occurs or becomes distinct. It is

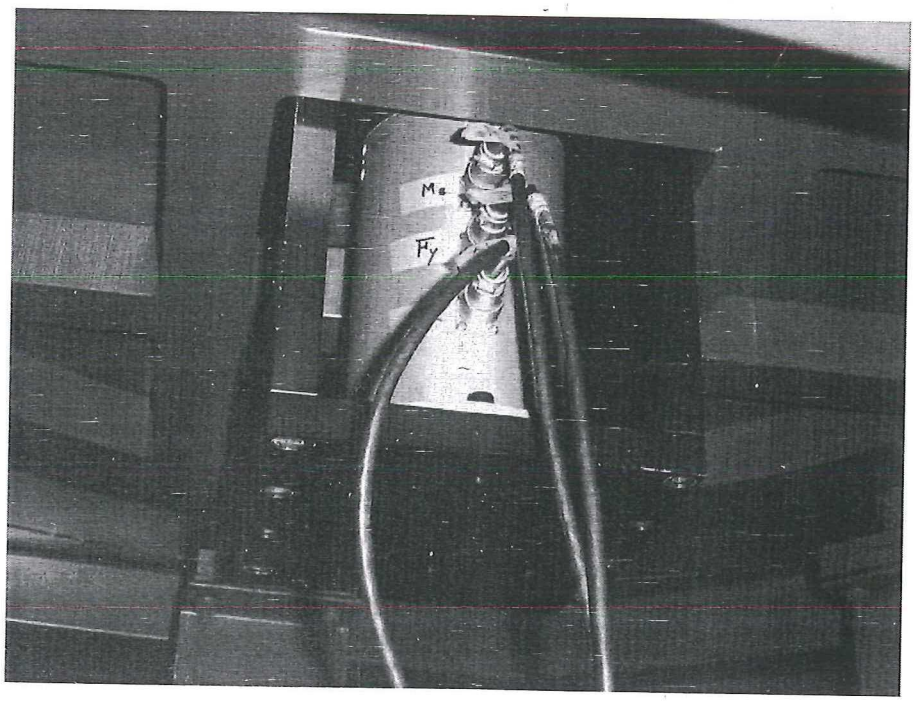

Fig. 7. 3-Component load cell to measure the forces on model sail.

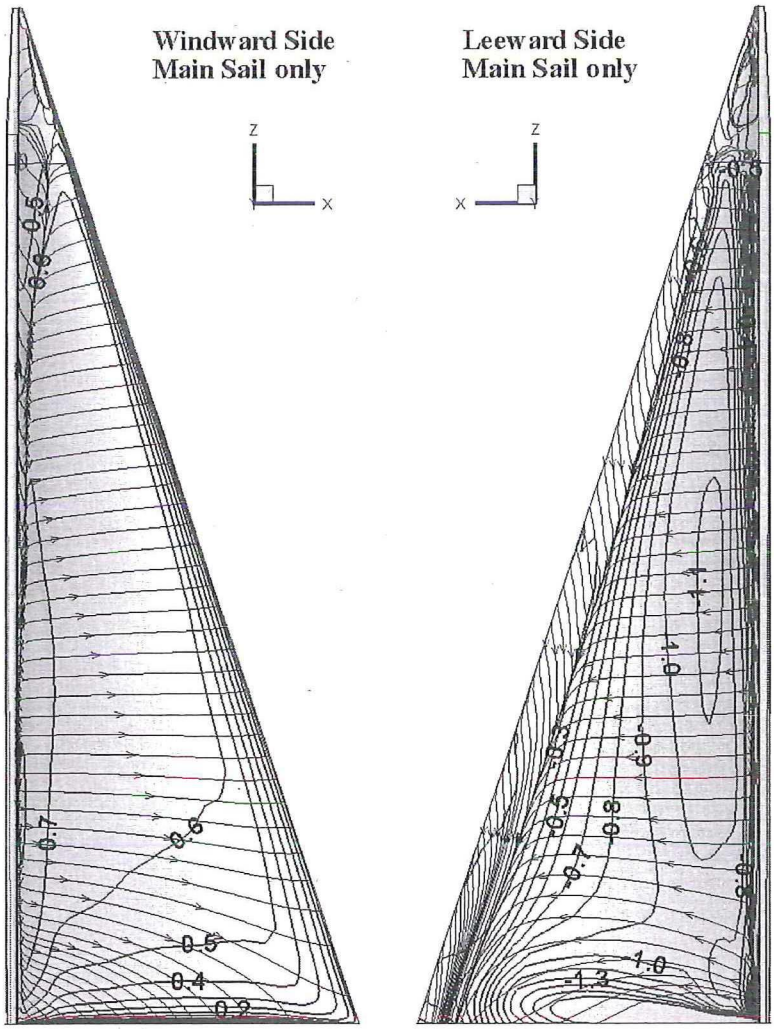

Fig. 8. Cp contours and limiting streamlines on main sail with no interactions.

mainly due to the downwash induced by the main sail close to the trailing edge of the jib sail. Such the flow separation could be observed on the windward side of the main sail due to the upwash under the existence of the jib sail as the mast angle reduces. For the extreme case of $\Phi_0 = 5°$, the upwash makes the effective inflow angle to the main sail negative, thus relatively large area of flow separation on the main sail occurs. The limiting streamlines on the sail surfaces are shown in Fig. 13, the peculiar pattern due to the phenomena of three-dimensional flow separation could be easily identified and the lines of detachment on the surface are more obvious as the gap distance reduces.

The lift and drag are computed for the above three cases. Fig. 14 shows the calculated and measured values of the lift coefficient. Due to downwash or upwash of each sail, the lift force changes from the case that the sails stand separately without any interactions. The lift force of the main sail reduces due to the upwash from sail interaction and this reduction becomes more significant as the gap distance decreases. But the change of the drag force is reversed in tendency as shown in Fig. 15. As the gap distance reduces, the drag of the main sail reduces, while the drag of the jib sail increases. However, the drag force for the combined main and jib sails and the sum of the drag forces for the two separate sails has

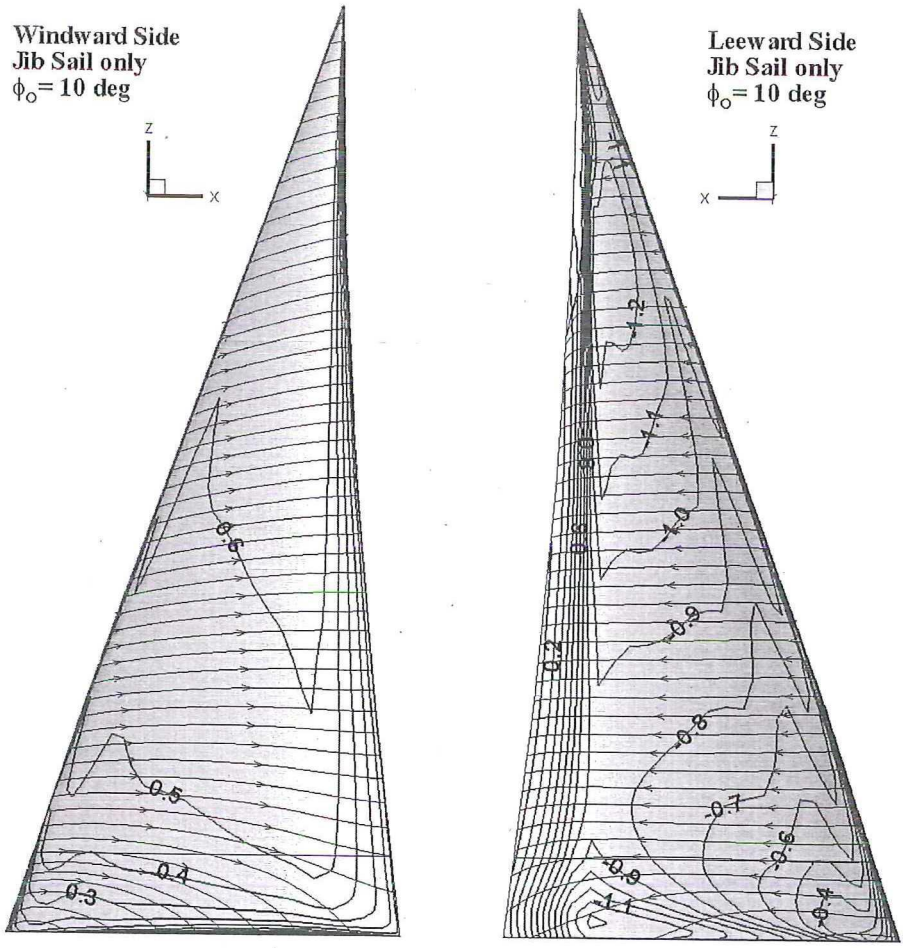

Fig. 9. Cp contours and limiting streamlines on jib sail with no interactions ($\Phi_0 = 10°$).

nearly the same value. The experimental results show reasonably good agreement with the calculations in tendency, although the values are not very close. The reason for the discrepancy in aerodynamic force between the calculation and the measurement can be explained as follows: (a) In the experiments some rigs including a boom and shrouds to

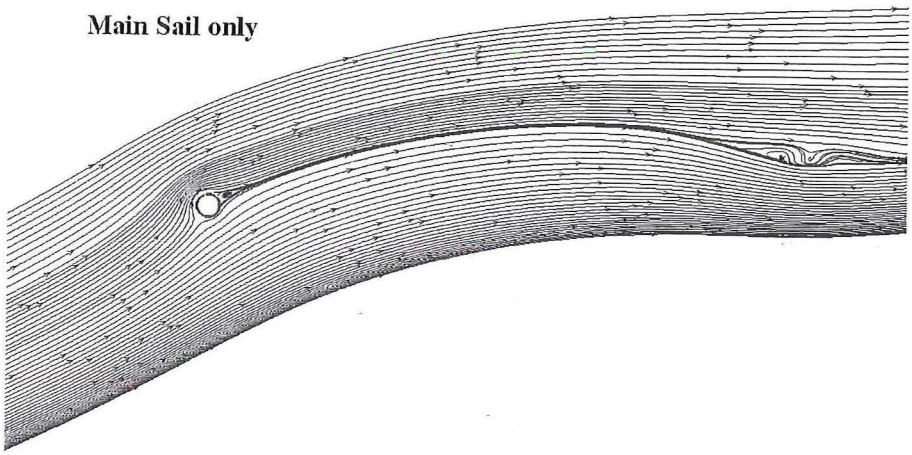

Fig. 10. Streamlines over main sail with no interactions (on the section of 25% height).

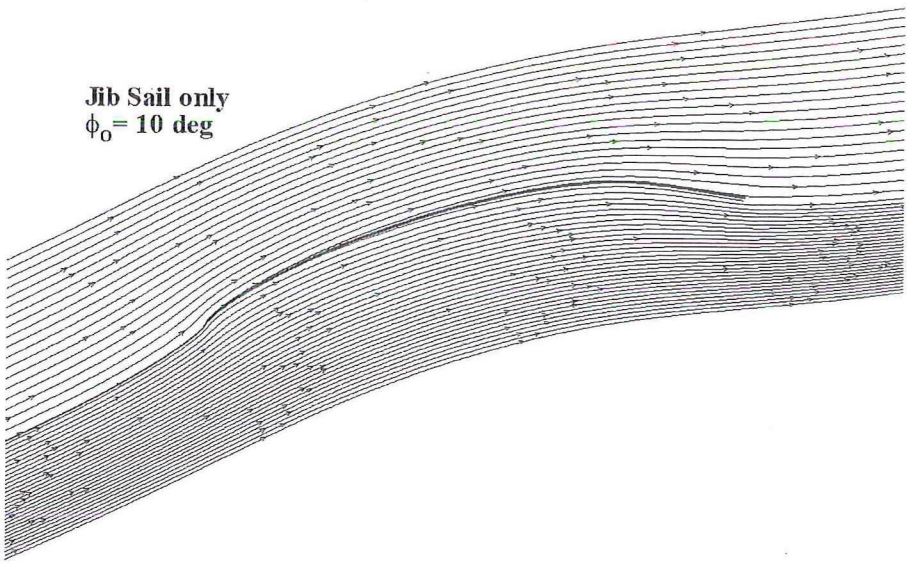

Fig. 11. Streamlines over jib sail with no interactions (on the section of 25% height, $\Phi_0 = 10°$).

support mast and sails are arranged to support the mast and the sails, but they are not in the present CFD calculation. It could provide an additional drag in experiments. (b) The scale effect exists due to the difference of Reynolds number between the calculation and the experiment. The Reynolds number for the model testing is much lower than that for the calculation and it could make the lift and drag of the model higher than the calculation. (c) The experiment must be performed in different environments for model sails compared to the case of the calculation in regarding sail-bottom and sail-model deck plate interaction and restricted wall effect in wind tunnel.

Fig. 16 shows the estimated full scale thrust force, i.e. the force component in the direction of vessel running. It is easily found that total thrust of sails increases when two sails combined properly than when they stand separately.

6.3. Center of effort (CE)

The location of CE is calculated to find the center of aerodynamic force acting on the sail surface. For the initial stage of yacht design, designer has to verify the location of center of sail force, center of effort (CE), and the center of hydrodynamic force on wetted body, which is normally called the center of lateral resistance (CLR), which is determined by the hull form and the arrangements and shapes of keel and other appendages. If it is failed, the yacht on sailing has to be experienced the undesirable helm forces by the moment due to the unbalance arm by discrepancy of two locations. Normally, most of designers use the empirical method to obtain the CE location, which is based upon the assumption that the center of aerodynamic force is the same as the center of projected area of the sail. A typical method for determining the location of CE is: One first determines the geometric centers of area of the main and jib sails. Then the line joining these two points is divided into two parts, by a simple geometrical construction, in proportion to the areas of each sail (Marchaj, 1996).

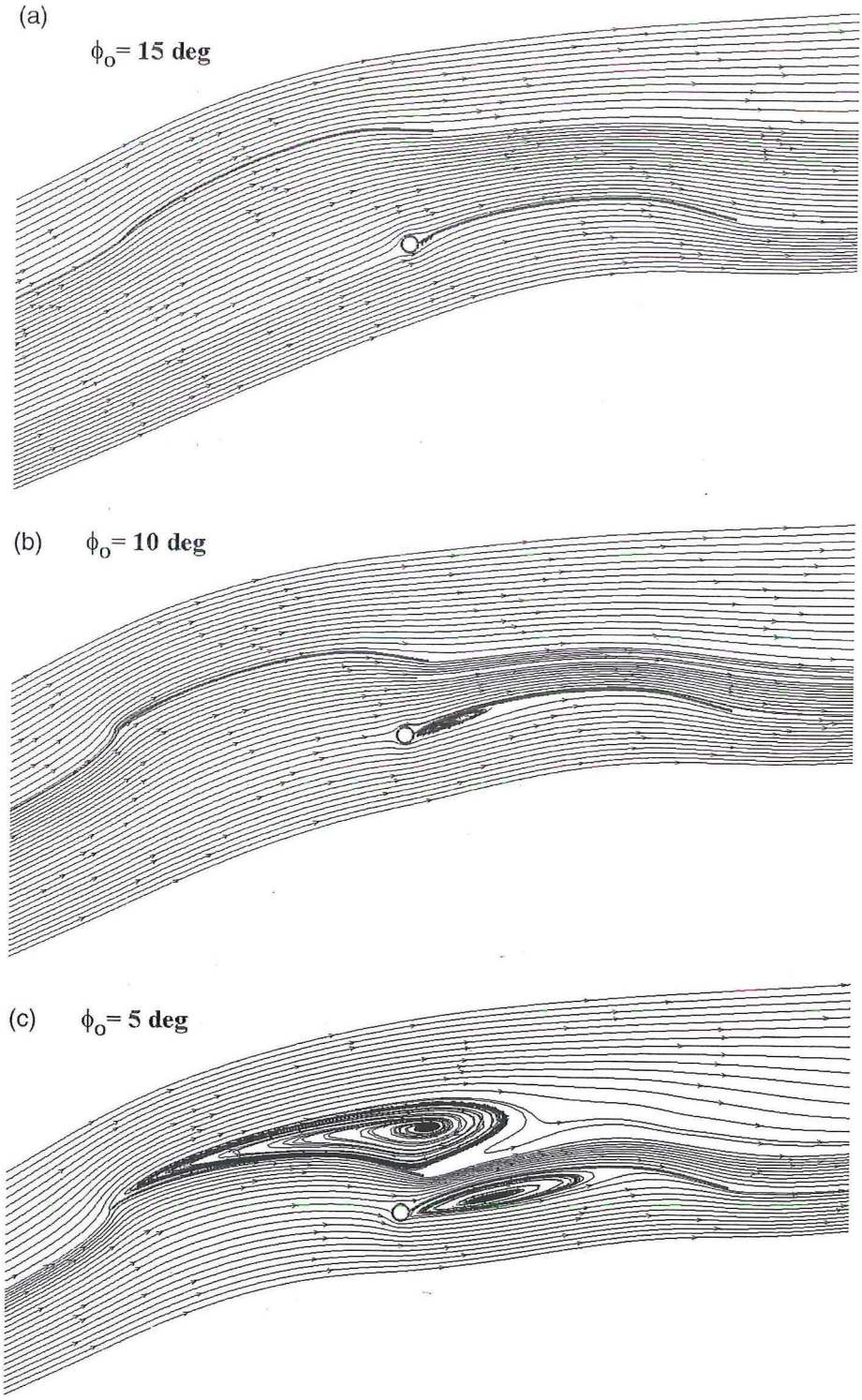

Fig. 12. Streamlines according to gap distance (on the section of 25% height) (a) $\Phi_0=15°$ (b) $\Phi_0=10$ (c) $\Phi_0=5°$.

In this paper, it is tried to calculate the location of the center of aerodynamic forces through the CFD. The location of CE can be obtained by finding the center of integrated aerodynamic forces on the sail surface. Table 3 shows the result of CE finding by the present CFD calculation with comparison of that by the empirical method. The calculation

is carried out for the condition of $\Phi_0 = 10°$ for jib sail. These two methods give some different result, which is thought to be not so significant in the reason that the errors in fixing the CE are partly compensated with similar errors arising in determination of the CLR. Typically, the location of CLR is also determined by simple geometrical center of

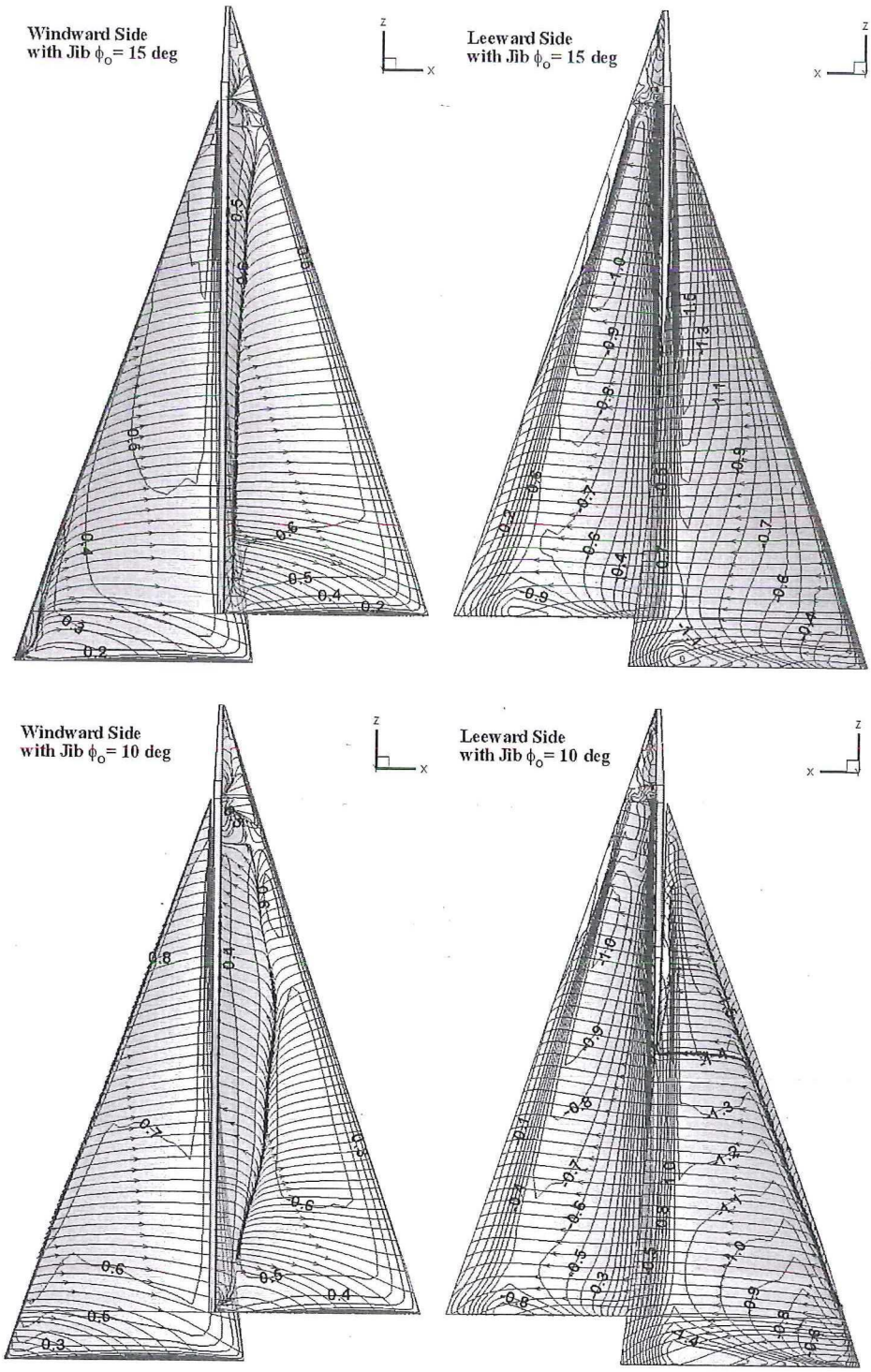

Fig. 13. Cp contours and limiting streamlines according to gap distance.

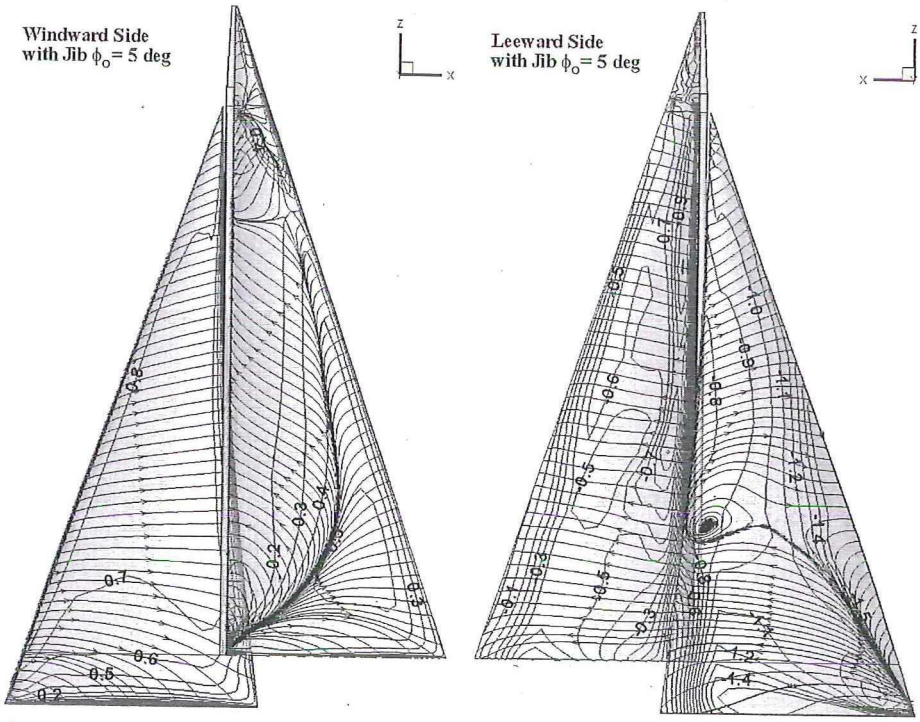

Fig. 13 (*continued*)

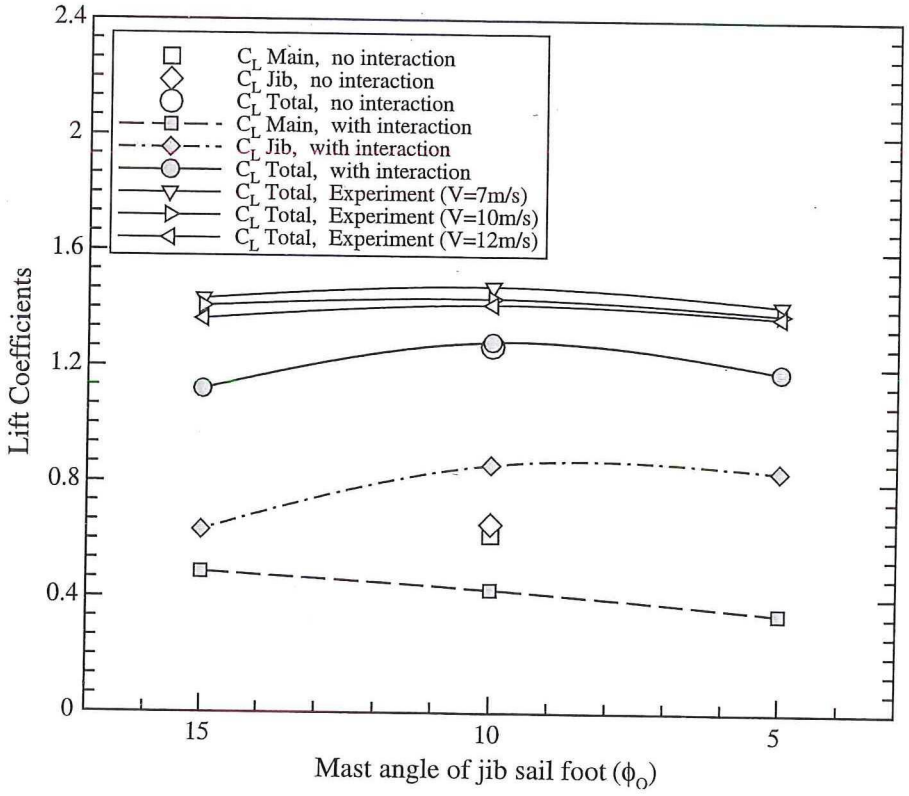

Fig. 14. Lift coefficients according to gap distance.

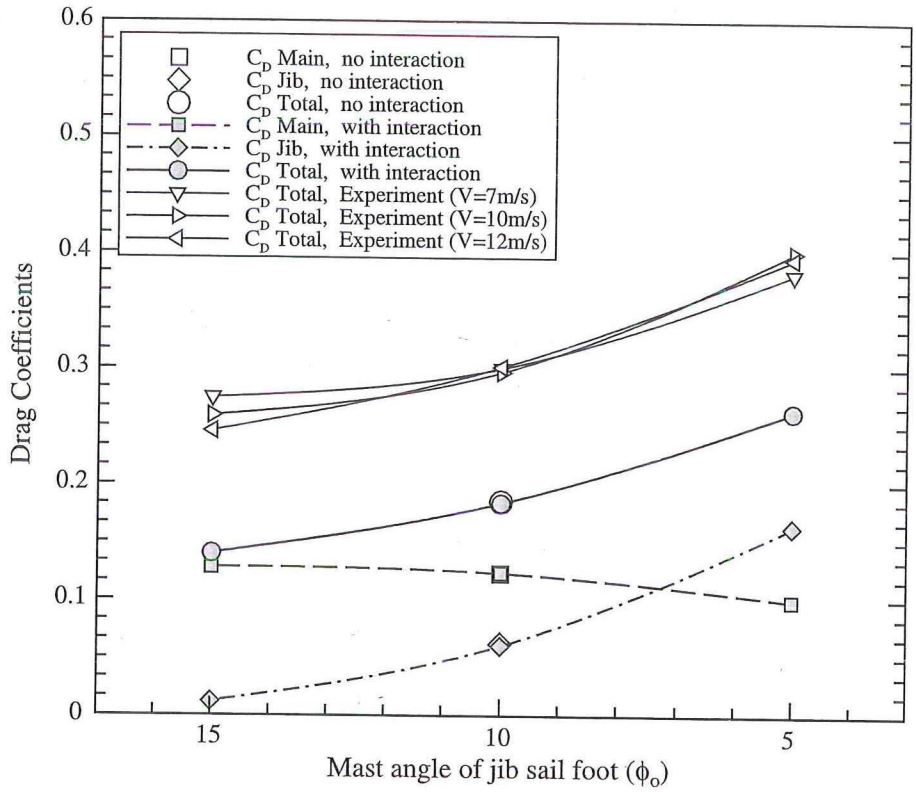

Fig. 15. Drag coefficients according to gap distance.

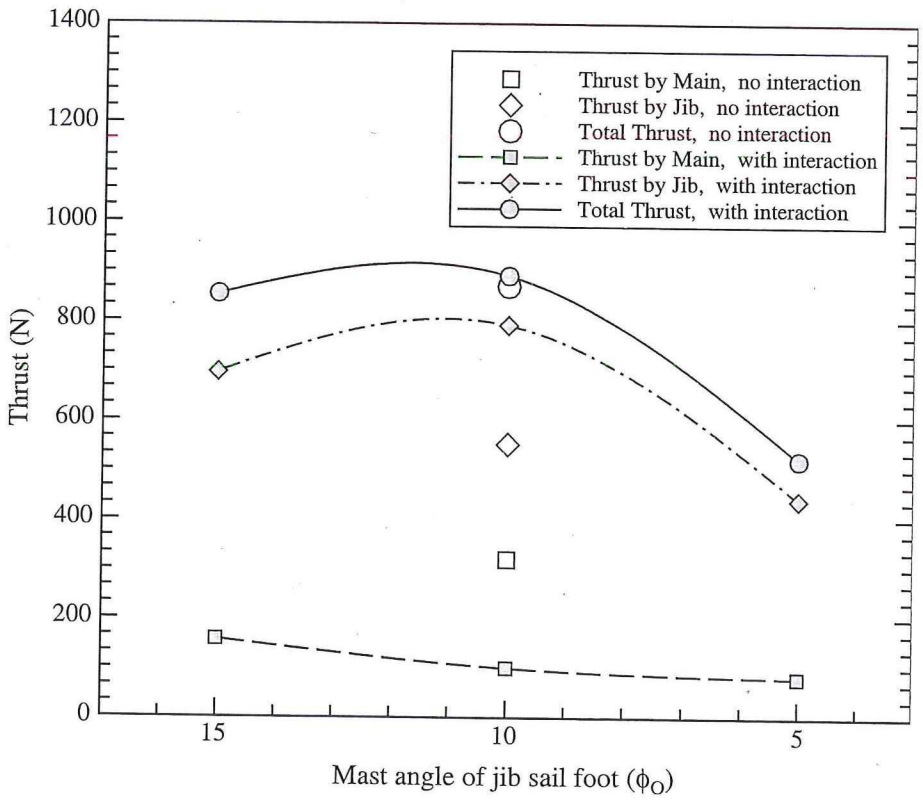

Fig. 16. Thrust according to gap distance.

Table 3
Calculated location of *CE*'s

	Present (mm)	Empirical (mm)	Difference
Longitudinal	−341.6	−130.9	210.7
Vertical	3592.9	3312.7	280.2

CE locations are measured based on origin (tag of main sail).

area of under water body. It can be suggested that CFD technique can be a most useful method for finding CE and it could be a better way for finding CLR in near future.

7. Summary and conclusions

The finite volume based multi-block RANS code, is applied to simulate turbulent flows around the sail system of a 30 feet sloop. For the application, the viscous flow phenomena and aerodynamic forces are predicted for practical sail-like wings at the real-scale Reynolds number. The computed results show reasonably good agreement in tendency with the experimental data obtained from the wind tunnel test using FRP sail models.

It is found that when the two sails are combined appropriately, larger lift forces can be produced than the case that two sails stands separately. By interaction between two sails, particularly the main and jib sails, it is found certain that most of the effective thrust comes from the jib sail. Broadly, there are two schools of thought: those who maintain that the jib sail accelerates the air past the leeward side of the main sail increasing the suction; those who argue that the function of the fore sail is as a sail in its own right and a very efficient one at that (Marchaj, 1996). Just with the results of the studies on this paper, the later opinion seems to be more reasonable. Whidden and Levitt, (1990) has been shown the jib sail is more effective than the main sail. It is because the circulations of main and jib sails tend to oppose and cancel each other in the area between the two sails and therefore more air is forced over the lee side of the jib. It is a kind of downwash on jib sail, which makes the angle of attack of apparent inflow to the jib sail be increased. Also one more reason is that the jib causes the stagnation point of the main sail to shift toward the leading edge of the mast, placing the main sail in a header due to downwash, but it is thought less effective to total thrust increment.

It is noteworthy that the cost effectiveness and the level of flow details provided by CFD tools are drawing much attention for the shape design of sail system and control guidance, considering that all the computations for the present study are carried out in a PC and the CPU time required for 1.8 million grids is about 16 h to get fully converged solution. It is quite certain that CFD can be a very powerful and useful tool for the aero- and hydro-dynamic performance prediction of sailing yacht in basic design stage.

References

Abbott, I.H., Doenhoff, A.E.V., 1949. Theory of Wing Sections. Dover Publications, New York.

Claughton, A.R., Campbell, I.M.C., Nov. 1994. Wind tunnel testing of sailing yacht rigs, 13th International Symposium on Yacht Design and Yacht Construction, Amsterdam.

Claughton, A.R., Wellicome, J.F., Shenoi, R.A., 1998. Sailing Yacht Design. Addison Wesley Longman Limited, England.

Ferziger, J.H., Peric, M., 1999. Computational Methods for Fluid Dynamics, second ed. Springer, Berlin.

Kim, W.J., Van, S.-H., 2000. Comparisons of turbulent flows around two modern VLCC hull forms, Proceedings of a Workshop on Numerical Ship Hydrodynamics, Gothenburg, Sweden.

Kim, W.J., Kim, D.H., Van, S.-H., 2002. Computational study on turbulent flows around modern tanker hull forms. International Journal for Numerical Methods in Fluids 38 (4), 377–406.

Launder, B.E., Spalding, D.B., 1974. The numerical computation of turbulent flows. Computer Methods in Applied Mechanics and Engineering 3, 269–289.

Lee, Y.W., Miyata, H., Sato, T., 1997. CFD simulation of two-sail interaction about a sailing Yacht. Journal of the Society of Naval Architect, Japan, 25–34.

Marchaj, C.A., 1996. Sail Performance (Theory and Practice). Adlard Coles Nautical, London.

Rhie, C.M., Chow, W.L., 1983. A numerical study of the turbulent flow past an isolated airfoil with trailing edge separation. American Institute of Aeronautics and Astronautics Journal 21, 1525–1532.

Shih, T.-H., Liou, W.W., Shabir, A., Zhu, J., 1995. A new eddy viscosity model for high Reynolds number turbulent flows—model development and validation. Computers and Fluids 24, 227–238.

Stone, H.L., 1968. Iterative solution of implicit approximations of multidimensional partial differential equations. SIAM Journal of Numerical Analysis 5, 530–558.

Van Doormal, J.P., Raithby, G.D., 1984. Enhancements of the SIMPLE method for predicting incompressible fluid flows. Numerical Heat Transfer 7, 147–163.

Whidden, T., Levitt, M., 1990. The Art and Science of Sails. ST. Martin's Press, New York.

Wilkinson, S., 1989. Static pressure distributions over 2D mast/sail geometries. Marine Technology 26 (4), 333–337.

Yoo, J., et al., 2005a. Calculations on the interactions between main and jib sails. Journal of the Society of Naval Architects of Korea 42 (1), 24–33.

Yoo, J., et al., 2005b. Development of 30 feet sailing yacht and performance predictions. Journal of the Society of Naval Architects of Korea 42 (1), 34–42.

Yoo, J., et al., 2005c. Experimental study on the hydrodynamic forces of 30 feet sailing yacht. Journal of the Society of Naval Architects of Korea 42 (3), 233–240.